Supplementary Materials for

Potassium channel dysfunction in human neuronal models of Angelman syndrome

Alfred Xuyang Sun*†, Qiang Yuan*, Masahiro Fukuda, Weonjin Yu, Haidun Yan, Grace Gui Yin Lim, Mui Hoon Nai, Giuseppe Alessandro D'Agostino, Hoang-Dai Tran, Yoko Itahana, Danlei Wang, Hidayat Lokman, Koji Itahana, Stephanie Wai Lin Lim, Jiong Tang, Ya Yin Chang, Menglan Zhang, Stuart A. Cook, Owen J. L. Rackham, Chwee Teck Lim, Eng King Tan, Huck Hui Ng, Kah Leong Lim, Yong-Hui Jiang, Hyunsoo Shawn Je†

*These authors contributed equally to this work.
†Corresponding author. Email: sunxya@gis.a-star.edu.sg (A.X.S.); shawn.je@duke-nus.edu.sg (H.S.J.)

Published 20 December 2019, *Science* **366**, 1486 (2019)
DOI: 10.1126/science.aav5386

This PDF file includes:

Other Supplementary Materials for this manuscript include the following:
(available at science.sciencemag.org/content/vol/366/6472/1486/DC1)

Movies S1 to S4 (.mov)
Tables S1 to S5 (.xlsx)

Materials and Methods

hPSCs Cell Culture

Human ESC lines H1 and H9 were originally obtained from WiCell Research Institute (Madison, WI), and have been maintained in the laboratory. AS iPSC was obtained from Kerafast (AG1-0). All hESC and hiPSC lines were cultured in mTeSR1 media (Stemcell Technologies) under feeder-free conditions in matrigel-coated cell culture plates and were routinely passaged (1:100) using Versene (Thermofisher). All lines displayed normal karyotypes.

Animals

Transgenic mice used in present study were originally generated by the Beaudet's lab and backcrossed more than 10 generations with C57BL/6J (*4*). We obtained the mice from the lab of Yong-Hui Jiang (Duke University, USA). All experiments related to animals were conducted following the protocol approved by the Institutional Animal Care and Use Committee (IACUC) of SingHealth. Mice were housed in SPF rooms with a 12-hour light/dark cycle. Wild-type (*Ube3a*$^{m+/p+}$) and maternal knockout (*Ube3a*$^{m-/p+}$) mice were produced from breeding of *Ube3a*$^{m+/p-}$ females and *Ube3a*$^{m+/p+}$ males. Genotyping was conducted by using primers: P1: 5' –AAC TTC ACT GCT ACA TCT CCA TGG C; P2: 5' –GCT CAA GGT TGT ATG CCT TGG TGC T; P3: 5'-TGC ATC GCA TTG TCT GAG TAG GTG TC.

Generation of UBE3A KO hESCs

A single guide RNA (sgRNA) was designed using the online Benchling design tool (https://benchling.com), targeting exon 6 of human *UBE3A* gene. sgRNA sequence is: 5'-CTACTACCACCAGTTAACTGAGG-3' and was cloned into lenti-CRISPR v2 (Addgene, #52961) as previously described (*32*). 5 µg of Cas9-sgRNA expression plasmid were used to transfect into human ESCs (1 x 10^6 cells) using nucleofection kit (Lonza). Next day, cells were selected by puromycin (500 ng/ml) for 2 days, followed by dissociation into single cells and were replated at low density on a matrigel-coated plate with mTeSR1 medium (Stemcell Technologies). Single hESC clones were picked and split into 2 batches (one for genotyping and the other for maintenance). Targeted *UBE3A* locus were amplified using REDiant Taq DNA polymerase (First base, Bio-5115-500U). PCR products were analysed by Sanger sequencing.

Generation of induced neurons from hPSCs

hPSCs were induced to neurons as previously described (*11, 33)*. Briefly, hESCs and hiPSCs were dissociated with TrypLE Express (Thermofisher) to single cells and plated onto matrigel coated cell culture plates in mTeSR1 media supplemented with thiazovivin (1 µM, Tocris). Next day, cells were transduced with lentiviruses expressing tet-mNgn2 and rtTA. In the following day, culture media was completely replaced with Neuronal Media (Sciencell) supplemented with doxycycline (1 µg/ml) for the next 5 days. Cells were selected with puromycin (3 µg/ml) for 48 hours starting day 3 to enrich for transduced cells. At day 5, cells were dissociated to single cells by TrypLE Express (Thermofisher) and replated onto either matrigel-coated glass coverslips (for immunostaining, AFM, and electrophysiological recordings) or 10cm cell culture plates (for biochemical assays) in BrainPhys media (Stemcell Technologies) supplemented with SM1 (1X, Stemcell Technologies) and Antibiotic-Antimycotic (1X, Thermofisher). Primary rat glial cells were added onto human induced neuronal cultures at day 7. Neurotrophic factors (BDNF, GDNF, NT3, each at 10 ng/ml, all from PeproTech) and 1% FBS and FUdR (5-

fluorodeoxyuridine: 16.5 mg/ml, Sigma F0503, with Uridine: 6.7mg/ml, Sigma U3003) were added starting day 10 until the day of analyses.

Generation of cortical organoids from hPSCs

Cortical organoids were generated based on a published protocol (*23*) with minor modifications. hPSCs were dissociated to single cells by TrypLE Express (Thermofisher) and seeded into U-shaped ultra-low attachment 96-well plate (Corning) at a density of 6K cells/well in the presence of thiazovivin (5 μM, Tocris). After spheroid formation, media were completely changed to Neural Induction Media (NIM: DMEM/F12 (Nacalai Tesque), 20% KnockOut Serum Replacement (Thermofisher), 1% minimum essential media-nonessential amino acid (Thermofisher), 1% GlutaMax (Thermofisher), 1% Antibiotic-Antimycotic (Thermofisher), 0.1% β-mercaptoethanol (Thermofisher), 5 μM Dorsomorphin (Tocris), 10 μM SB431542 (Stemgent)) for the next 6 days, with media change every other day. Starting day 7, media were changed to Neural Growth Media (NGM: Neurobasal (Thermofisher), 1:50 B27 without vitamin A (Thermofisher), 1% GlutaMAX (Thermofisher), 1% Antibiotic-Antimycotic (Thermofisher), 20 ng/ml EGF (PeproTech), 20 ng/ml FGF-basic (PeproTech)) for the next 18 days, with media change every other day. Starting day 25, organoids were transferred out of 96-well plates to 6-well plates (6-8 organoids per well), cultured in Organoid Media I (OMI: Neurobasal (Thermofisher), 1:50 B27 without vitamin A (Thermofisher), 1% GlutaMax (Thermofisher), 1% Antibiotic-Antimycotic (Thermofisher), 10 mM HEPES (Thermofisher), 10 ng/ml BDNF (PeproTech), 10 ng/ml NT3 (PeproTech)) until day 100 on an orbital shaker (75 rev/min). After day 100, media were changed to Organoid Media II (OMII: BrainPhys (Stemcell Technologies), 1:50 SM1 (Stemcell Technologies), 1% GlutaMax (Thermofisher), 1% Antibiotic-Antimycotic (Thermofisher), 10 mM HEPES (Thermofisher), 10 ng/ml BDNF (PeproTech), 10 ng/ml GDNF (PeproTech), 10 ng/ml NT3 (PeproTech), 100 μM db-cAMP (Sigma)).

Production of 3rd generation lentiviral particles

To generate lentiviral particles, lentiviral expression vectors (tetO-NGN2-Puro: Addgene#52047; FUW-rtTA: Addgene#20342) together with helper plasmids (pMDLg/pRRE: Addgene#12251; pRSV-Rev: Addgene#12253; pMG2.G: Addgene#12259) were cotransfected into Lenti-X 293T cells (Clontech) using Fugene HD (Roche). Supernatants were collected from culture media and lentiviral particles were concentrated using Lenti-pac concentration solution (GeneCopoeia).

Gene Expression Analyses

For quantitative RT-PCR analyses of human neurons, total RNA was extracted using DirectZol (Zymo), treated with DNAse, and converted to cDNA using High Capacity cDNA Reverse transcription kit (Life Technologies). Real-time PCR assay was performed using the Applied Biosystems 7900HT Fast real-time PCR system. Primers sequences used in the study was included in Table S5.

Fluorescent Immunocytochemistry

hESCs or induced neurons were fixed with 4% paraformaldehyde (PFA) in PBS for 15 minutes, permeabilized with 0.25% triton X-100 in PBS for 15 minutes and blocked by blocking buffer (5% BSA and 1% FBS in PBS) for 60 mins. Next, samples were incubated with primary antibodies (chicken anti MAP2: Abcam AB5392, rabbit anti Synapsin I: SYSY 106103, mouse anti UBE3A: SIGMA E8655, rabbit anti UBE3A: SIGMA HPA039410) 2 hours in room

temperature (RT) or overnight at 4 °C. Samples were incubated with secondary antibodies for 1 hour in RT and mounted on glass coverslips. Images were acquired using an LSM 710 (Zeiss) confocal microscope. Quantifications (synaptic boutons, neuronal complexities, etc.) were done using a MetaMorph software.

Organoids were fixed in 4% PFA in PBS overnight, washed in PBS, incubated in 30% sucrose in PBS at 4°C overnight, and subsequently embedded in O.C.T. (Sakura Finetek). Fixed organoid samples were cryosectioned using a cryostat (Leica). For immunofluorescence, cryosections were washed with PBS to remove excess O.C.T compound and blocked with 3% BSA and 0.5% Triton X-100 in PBS for 1 hr. at RT. Sections were incubated with diluted primary antibodies overnight at 4°C and secondary antibodies for 1 hr. at RT. All sections were counterstained with DAPI (Sigma-Aldrich) and mounted with FluorSave media (Millipore). Images were taken on an LSM 710 (Zeiss) or TCS SP8 (Leica) confocal microscopes. The following primary antibodies were used: chicken anti MAP2 (Abcam AB5392), mouse anti NeuN (Millipore MAB377), rabbit anti BRN2 (GeneTex GTX114650), rabbit anti TBR2 (Abcam AB23345), rat anti CTIP2 (Abcam AB18465), mouse anti CUX1 (Abnova H00001523-M01), rabbit anti GABA (Sigma A2052), mouse anti GFAP (Milipore MAB360).

Electrophysiology

Whole cell patch clamp recordings were performed on induced neurons in RT as described previously (*33*). Recording pipettes with resistances of 4–6 MΩ were filled with internal solution containing (in mM): 135 $KMeSO_3$, 10 KCl, 1 $MgCl_2$, 10 HEPES, 2 Na_2ATP, 0.4 Na_3GTP with osmolarity of 290 mOsm and pH 7.3~7.4. Neurons were bathed in the extracellular solution containing (in mM): 140 NaCl, 3 KCl, 10 dextrose, 2 $MgCl_2$, 2.5 $CaCl_2$, 10 HEPES at pH 7.3-7.4. Neuronal intrinsic excitability was measured in the presence of CNQX (20 μM, Tocris) and APV (50 μM, Tocris) to block all excitatory synaptic responses. Recording was sampled at 40 kHz and filtered at 2 kHz (Digidata 1440A, Molecular Devices). We only chose pyramidal-shaped, similar-sized neurons based on their capacitance measurements. Data with serial resistance higher than 20 MΩ or leaking current more than 200 pA were rejected. Resting membrane potential was estimated in current-clamp mode immediately after breaking into the membrane and establishing whole-cell configuration. For analysis of parameters of action potentials evoked by stepped current injection (500 ms duration, 20 pA stepwise from -20 pA to +360 pA with 4 s interval) under current clamp model. Stepped voltage depolarization (500 ms duration, 20 mV stepwise and 10 steps with 4 s interval) was performed to obtain voltage-gated sodium and potassium currents as well as pharmacological isolation of BK currents (fig. S2A).

Whole cell patch clamp recordings of neurons in the organoid (wholemount) and acute mouse hippocampal slices were performed in a recording chamber (RC-26GLP, Warner Instruments) and submerged under continuously perfused artificial CSF (aCSF) containing (in mM): 119 NaCl, 2.5 KCl, 11 glucose, 26 $NaHCO_3$, 1.25 NaH_2PO_4, 2.5 $CaCl_2$ and 2 $MgCl_2$ saturated with 95% O_2 and 5% CO_2 at 30-32 °C. Neuronal intrinsic excitability was measured in the presence of CNQX (20 μM, Tocris) and APV (50 μM, Tocris) to block all excitatory synaptic responses. We targeted neurons near the surface of organoids with reasonably pyramidal-shaped cell bodies under our DIC/IR camera. Patch glass pipettes (3-4 MΩ) were filled with an intracellular solution containing (in mM): 135 $KMeSO_3$, 10 KCl, 10 HEPES, 1 EGTA, and 2 Na_2ATP. The osmolality was adjusted to 290 mOsm, and the pH was adjusted to 7.3-7.4. The whole cell recordings were performed using an Olympus BX51WI upright microscope equipped with a 60x water-immersion lens with DIC-IR. Signals were recorded

using a MultiClamp 700B amplifier, filtered at 2 kHz using a Bessel filter, and digitized at 40 kHz with a Digidata 1550B analog-to-digital (A/D) board (Molecular Devices, Sunnyvale, CA). Resting membrane potential was estimated in current-clamp mode immediately after breaking into the membrane and establishing whole-cell configuration. To test neuronal excitability, a series of current pulses (500 msec) of increasing amplitude from 0 pA to +35 pA (in 5 pA increment, 4 s interval) for organoid neurons and from 0 pA to +240 pA (in 10 pA increment, 4 s interval) for mouse neurons, respectively, were injected to obtain the frequency-current injection (F-I) curve.

For fAHP analysis in all recordings, automatic detection and calculation was conducted by customized matlab scripts adapted from published algorithm (*13,34-35*). Spikes threshold was defined as the time-point when membrane potential increasing slop equal to 5 mV/ms. The amplitude of the fast AHP (fAHP) was defined as the voltage difference between spike threshold and the lowest point in each given spike within 10 ms. The fAHP amplitude of each neuron was calculated by averaging the fAHP of the first spike in all current injection steps. We ran automated scripts to detect the threshold of action potentials and fAHPs in a blind-manner.

***In vivo* local field potential (LFP) recording in freely moving mice.**

Mice (10-12 weeks) were anesthetized with continuous isoflurane at the stereotaxic apparatus (RWD). Eye cream was applied to a mouse to protect the eye from drying due to anesthesia. 2% lidocaine was injected under the scalp and subsequently scalp was removed to expose the skull. The brachium of inferior colliculus (BIC) was located by the following coordinate: anterior-posteror (AP), -4.1 mm; Lateral, 2.1 mm; Depth, 2 mm, referring from Bregma. Stereotrodes were made with platinum-iridium wire (90%:10%, A-M system) and unilaterally implanted into BIC. Stainless steel screw (AP: 2 mm, Lateral: 2 mm) was used as a reference electrode. Iodopavidone was applied for disinfection around the surgical area after dental cement mounting. Mice were maintained on a heating pad at 37 ºC till waking up from the anesthesia before putting back to home cages. LFP recordings were performed on the mice 5 days after surgery. LFP recordings were conducted in a copper-Faraday chamber. For evoked LFP, auditory stimulus (~125 dB, 500 Hz) was provided by a speaker (EKX, Electro-Voice) driven by a customized program in Matlab. LFP was recorded with sampling rate at 500 Hz and filtered with 0.5 Hz high-pass and 100 Hz low-pass by EEG/EMG recording system (Pinnacle). Raw signals were converted by fast Fourier transform (FFT) to calculate power spectral density (PSD) using Matlab and NeuroExplorer. Video was recorded simultaneously for further analysis. After all recordings, mice were sacrificed, and their brains were isolated and fixed using 4% PFA in PBS and the implanted electrode locations were confirmed by either bright field imaging or DAPI staining and subsequent fluorescence imaging.

Biochemistry

Induced neurons or cortical organoids were lysed in RIPA buffer supplemented with protease and phosphatase inhibitor cocktails. Protein samples were loaded onto 8-12% Bis-TRIS (NP0322BOX Invitrogen) and were transferred onto a PVDF membrane. After blocking with 5% milk in TBS-T buffer for 1 hour, PVDF membranes were incubated with primary antibodies overnight at 4°C, followed by 1 hour incubation with secondary antibodies at RT. Images were visualized by either chemiluminescence or NIR fluorescent detection using c600 Imaging System (Azure Biosystems Inc). HEK293 cells were grown in DMEM (Sigma) containing 10% FBS (Gibco) and 100 U/mL penicillin-streptomycin (Gibco) in a 5% CO_2 incubator. Cells were

transfected with Lipofectamine PLUS (Invitrogen), subsequently were treated with 1 μM of MG132 (A.G Scientific) for another 24h. Next, cells were lysed in PBS containing 1% SDS (Invitrogen), 1mM PMSF (USB), 10 μg/ml aprotinin (Roche), and 1% (v/v) phosphatase inhibitor cocktail 2 and 3 (Sigma).

Co-IP in HEK293 Cells: HEK293 cells were transfected with either Flag-BK (Gift of Dr. Cang Yong, ZJU, China) and/or HA-UBE3A plasmids (Addgene #8658) using lipofectamine 3000 (ThermoFisher) and lysed in a buffer containing 1% Nonidet P-40, 150 mM NaCl and 50 mM Tris-HCl with 100 μM $CaCl_2$, 1X protein inhibitor (Roche), and 1X PMSF. Lysates were centrifuged for 15 mins at 4°C after 20-min incubation on ice. Collected supernatant was pre-washed with 50 μl mouse-IgG beads for 2 hours and subsequently incubated with 25 μl of FLAG-M2 agarose beads (A2220, sigma) overnight at 4°C. Beads were collected via brief centrifugation, washed, and boiled with LSD sampling buffer (Invitrogen) for western analysis.

Cell-based ubiquitination: HEK293 cells were transfected with HA-ubiquitin (K63R), Flag-BK plasmids with either myc-UBE3A-WT or myc-UBE3A-MT plasmid with lipofectamine 3000. MG132 (1μM) was added in the culture. Cells were collected 24 hours after transfection and subsequently lysed in a buffer containing 1% Nonidet P-40, 150 mM NaCl, 50 mM Tris-HCl and 5 μM iodoacetamide. Lysates were centrifuged at 13,500 rpm for 15 mins at 4°C after 20-min incubation on ice. Next, supernatants (400 μg of total protein) were used for each condition and these supernatants were incubated with 40 μl of FLAG-M2 agarose beads (A2220, sigma) overnight in a continuously rotating platform at 4°C. Agarose beads were collected via brief centrifugation, washed by the lysis buffer, and boiled with a LDS sample buffer (Invitrogen) for subsequent western analysis.

In vitro ubiquitination: HEK293 cells were transfected with BK expression constructs and lysed in a radioimmune precipitation assay buffer containing 1% Nonidet P-40, 0.1% SDS, 0.5% sodium deoxycholate, 150 mM NaCl, 1 mM PMSF, 10 μg/ml aprotinin and 1% (v/v) phosphatase inhibitor cocktail 2 and 3 (SIGMA) in PBS. Lysates were centrifuged, and BK proteins were immunoprecipitated with anti-FLAG M2 agarose beads. These beads were then resuspended in an assay buffer provided by the ubiquitination kit K-230 (Boston Biochem). *In vitro* ubiquitination was performed according to the manufacturer instructions.

Endogenous BK ubiquitination: Primary cortical neuronal cultures were used to assess endogenous ubiquitination of BK. Fast genotyping was done before the preparation of neuronal cultures. Briefly, tails of newborn pups (2-3mm) was collected and lysed by Tween-20 based lysis buffer with proteinase K at 55 ºC for 20 mins. Fast PCR was completed with protocol: denaturation (98 ºC, 7s)- annealing (60 ºC, 10s)-extension (72 ºC, 15s) for 30 cycles. Mice brains of the same genotype were pooled. Cortices were first dissected out and dissociated to single cells using Trypsin (0.25%, Invitrogen) supplemented with DNAase I (1mg/ml, Sigma). Cells were plated to 10cm dishes pre-coated with poly L-lysine (Sigma), and maintained in neuronal media consisting of Neurobasal medium, 1X B27 supplement, 1X Glutamax, and 1X penicillin-streptomycin (all from Invitrogen). At DIV13, neurons were treated with MG132 (1μM) for 18-24 hours. At DIV14, cells were lysed in lysis buffer containing 1% Nonidet P-40, 150 mM NaCl, 50 mM Tris-HCl, 50 mM NaF and 5 μM iodoacetamide. BK antibody (4μg, Alomone) and protein-A/G beads was added to the lysates and incubated overnight at 4 ºC. Next day, beads was collected and boiled with LDS sample buffer before western blotting. Antibodies used: rabbit-anti-BKα (Alomone, APC151), rabbit-UBE3A (SIGMA, E8655), rabbit-UBE3A (SIGMA,

HPA039410), rabbit-Flag (SIGMA, F7425), rabbit-HA (SIGMA), goat-HA (SIGMA), rabbit-Myc (Millipore).

Atomic Force Microscopy (AFM)

A BK-channel specific antibody targeting an extracellular epitope (APC151, Alomone) were conjugated on a functionalized AFM tip (shown in fig. S3E). Briefly, ozone plasma cleaned silicon nitride cantilevers (AFM tips) were dried after rinsing in ethanol and ultrapure water. This is followed by incubation in 4% 3-aminopropyltrimethylethoxysilane (3-APTES) for 2 hours at room temperature (RT). Next, tips with attached NH_2 groups were incubated in a NHS-PEG-NHS linker (2 mg/ml in methylene choride, Invitrogen) for 2 hours and subsequently with a BK-channel antibody (20 µg/ml, APC, Alomone) in PBS for 2 hours at RT. Functionalized tips were further treated with 1mg/ml glycine in PBS to quench free functional groups. Control tips were prepared by following the same protocol without antibody conjugation.

AFM force measurements were performed as previously reported (*36, 37*). Silicon AFM probes with a nominal spring constant of 0.03 N/m and a tip radius of 10 nm (MSCT-D, Bruker) were used in a Nanowizard II BioAFM (JPK instruments AG, Germany). Functionalized cantilevers were calibrated *in situ* by a nondestructive thermal tune method using the build-in function provided by the JPK SPM Control Software. Neurons were fixed with 4% PFA in PBS and blocked by 5% BSA in PBS for 30 mins before AFM measurements (neurons with reasonably pyramidal-shaped cell bodies were selected for AFM measurement). A maximum loading force of 0.1 nN, Z length of 5 µm and a constant speed of 2.0 µm/s were used to generate single-peak specific interaction force curves (single bond rupture) (shown in fig. S3F). Force mappings were carried out in a 1 μm^2 scan area (with 10 x 10 data points) and at least 3 random locations were probed in each cell. JPKSPM data processing software v.5 was used to analyze the raw data obtained from the aforementioned protocol. Control experiments were conducted to eliminate potential artifacts resulted from nonspecific interactions and to ensure that the measured forces resulted from specific interactions between cantilever coated receptors and the BK channels on cell surface. Probes without antibody were tested on WT neurons and functionalized probes were tested on glial cells (shown in fig. S3G).

RNA sequencing

Human neuron-rat astrocyte co-cultures at day 40 were lysed in TRIzol (Thermofisher) and total RNAs were extracted using a Direct-zol RNA miniPrep kit (Zymo Research). RNA integrity was verified using an Agilent RNA 6000 Nano Chip and samples with a RIN above 8 (Bioanalyzer, Agilent) were further processed. cDNA libraries were prepared using Truseq Stranded mRNA (Poly A selection) kit (Illumina) and sequenced on a Hiseq3000 platform (Illumina) in paired-end mode. Sequenced libraries were trimmed using cutadapt (v. 1.13) with parameters *--quality-base=33 -m 20* and adaptor pairs AGATCGGAAGAGCACACGTCTGAACTCCAGTCA and AGATCGGAAGAGCGTCGTGTAGGGAAAGAGTGT. Trimmed reads were processed using Xenome (v. 1.0.0) separating rat reads (aligning to *R. norvegicus* release Rnor_6.0) and human reads (aligning to *H. sapiens* genome release GRCh38.p10). Reads classified by Xenome as "human", "both" and "ambiguous" were merged together and carried forward in the analysis. Human reads were aligned again to the same genome using STAR (v. 2.5.2b) with the following parameters: *--outFilterMultimapNmax 20 --alignSJoverhangMin 8 --alignSJDBoverhangMin 1 --outFilterMismatchNmax 999 --alignIntronMin 20 --alignIntronMax 1000000 --alignMatesGapMax 1000000* (*38, 39*). Only uniquely mapping reads were used for counting.

Read counts were obtained at the gene level using featureCounts (v. 1.5.1) with the Ensembl release 92 human GTF and the following parameters: *-t gene -g gene_id -O -s 2 -J -T 8 -p –R*. Raw counts were imported in R (v. 3.4.3) (*40*). Counts were normalized (DESeq2 between-sample normalization), log-transformed and principal component analysis was performed to visualize any confounding effects. Batch effect removal was simulated using the combat function in the Bioconductor package sva 3.32.1 (*41*), showing that accounting for the replicate effect in the linear model correctly clusters samples by genotype along the first principal component. Differential gene expression analysis was performed with DESeq2 (v. 1.18.1) using the formula *~ replicate + condition* and the Wald test (*41-43*). Reported fold changes have been moderated using the *lfcShrink* function in DESeq2, setting an alpha value of 0.05 for independent filtering and using default parameters. Nominal p-value distributions were checked by plotting their frequency histogram, revealing a pathological underestimation of the variance of the null distribution by the Wald test. The variance was empirically estimated and P-values were recalculated using the R package fdrtool v 1.2.15 (REF Strimmer, K. 2008. A unified approach to false discovery rate estimation. BMC Bioinformatics 9: 303). Genes with a statistically significant difference (adjusted p-value < 0.05) were tested for Gene Ontology and KEGG Pathway overrepresentation using gProfileR (v 0.6.6), using all genes with at least 1 read in 1 sample as background and strong hierarchical filtering (*44*). All genes were also tested against the MSigDB C5 collection (Gene Ontology) for Gene Set Enrichment Analysis (GSEA) using fgsea (v 1.4.1)) with 10000 iterations (*45-47*) and the "stat" column from the DESeq2 results table as input.

Organoids Ca^{2+} two-photon imaging

Multiphoton imaging was performed using a custom-built multiphoton microscope (Bergamo, Thorlabs, VA), equipped with a resonant scanner, a piezo Z drive, and a water-immersion lens (CFI75 Apochromat 25XC W, Nikon, Japan). The light source (MaiTai eHP DeepSee, Spectra-Physics, CA) was running at 800 nm or 920 nm, and the green fluorescence was collected using a 525/50 nm bandpass filter (Chroma, VT). Cortical organoids were stained with 2 μM Fluo-4AM in the culture medium (BP Organoid Medium) for 45 minutes in 37 ℃ CO_2 incubator. Time-lapse images of volumetric (533 x 533 x 50 μm^3 or 265 x 265 x 50 μm^3) stacks were taken at 1.26Hz for 3 min. During imaging sessions, organoids were kept at 37 ℃ using a plate heater (TC-324C, Warner Instruments, CT). Following to baseline imaging, drugs (Paxilline: 10 μM; TTX: 2 μM) were added. 10 minutes after drug application, another session of imaging was performed. Images were analyzed and quantified using ImageJ (NIH) and MATLAB (Mathworks, MA) as previously reported (*26, 27*).

Behaviors

Flurothyl-induced seizures: Experiment was conducted following the protocol adapted from previous report (*7*). Mice (8-9 weeks, both males and females) were put into a 1-liter transparent plastic chamber for 1 min habituation. Subsequently, chamber was capped with sealed cover and flurothyl (10% in ethanol, Sigma) was perfused onto a piece of tissue paper hung in the chamber at a rate of 100 μl/min by using a programmable syringe pump (Harvard Apparatus). The first myoclonic seizure was defined by a short but obvious jerk of a neck and body due muscle contraction. Each trial was terminated when the mouse exhibited generalized seizure as a loss of postural control. Chamber was cleaned and the tissue paper was replaced before each new trial.

Picrotoxin-induced seizure: Mice were injected with picrotoxin (3 mg/kg, i.p., Tocris Bioscience) and placed into 1L beakers for 30 min observation with simultaneous video recordings. Seizure severity of mice are dependent on multiple variables such as picrotoxin dose, mice age, and their body weights. We performed dosage-response experiments with a dosage from 2-5 mg/kg of picrotoxin in wildtype mice and found that 3 mg/kg of picrotoxin was optimal to induce grade 2 level seizure in wildtype mice. Videos were recorded for all the behavioral experiments. Behavioral analysis was performed in a double-blind manner with littermates (siblings of wild-type (*Ube3a*$^{m+/p+}$) and maternal knockout (*Ube3a*$^{m-/p+}$) mice that produced from same pairs of *Ube3a*$^{m+/p-}$ females and *Ube3a*$^{m+/p+}$ males).

Figure S1

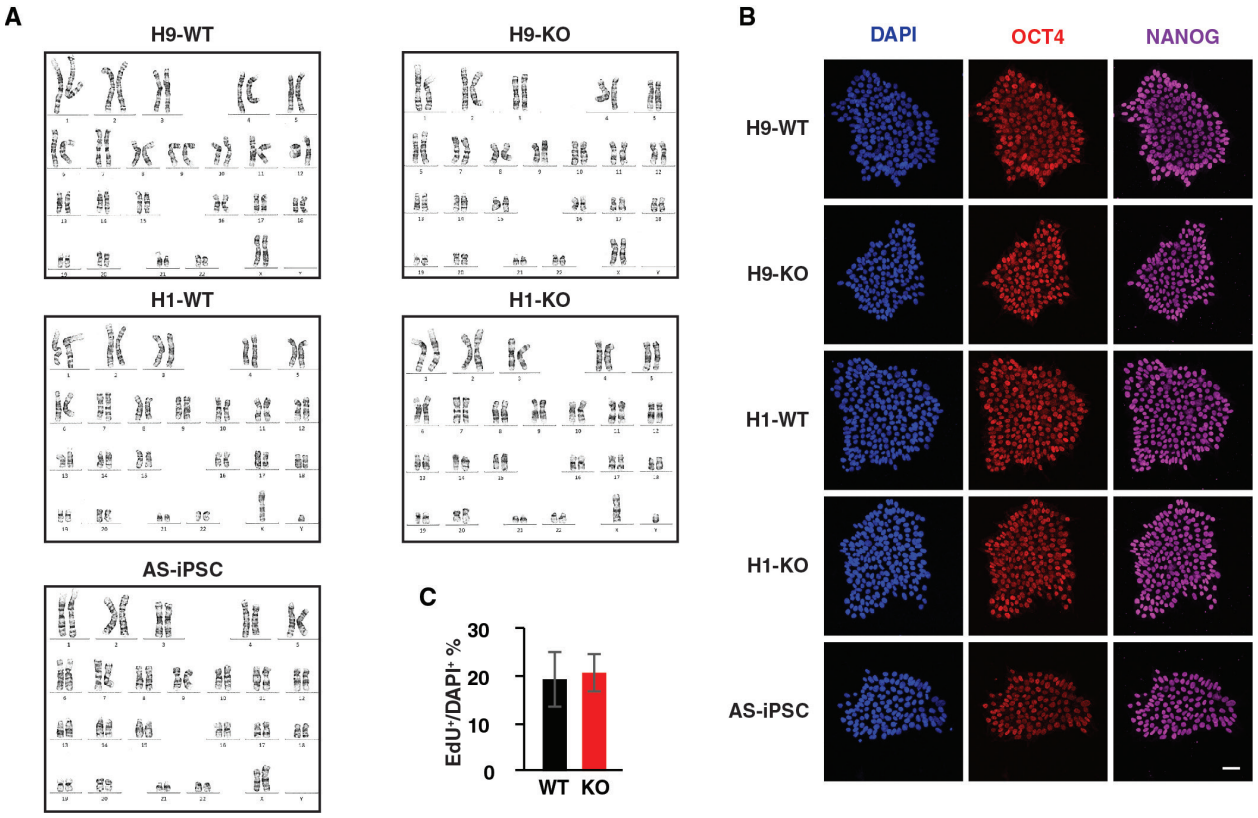

Fig. S1. Characterization of human embryonic stem cells (hESCs) and AS-patient derived iPSCs.

(**A**) Normal karyotypes of hESCs and hiPSC lines used in the study. (**B**) Immunostaining with specific antibodies against pluripotency markers (OCT4 and NANOG) in hESCs and iPSCs. Scale bar: 50 μm. (**C**) Quantification of proliferating cells in WT and KO hESCs. Cells were pulse-labeled with EdU for 3 hours before immunostaining. N = 4 independent batches. Data represent mean ± SEM.

Figure S2

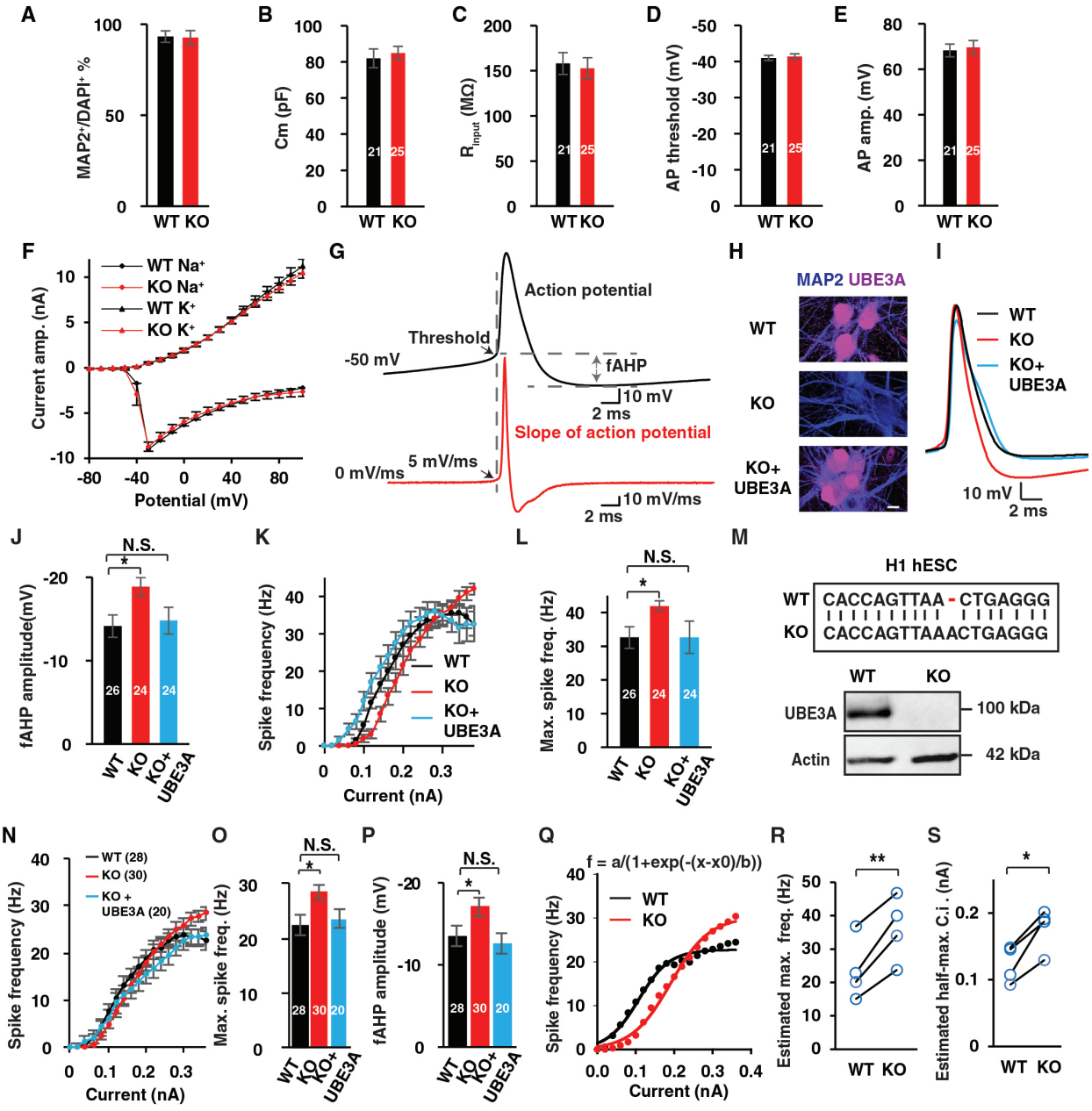
A
MAP2+/DAPI+ %
WT KO
B
Cm (pF)
C
R_input (MΩ)
D
AP threshold (mV)
E
AP amp. (mV)
F
WT Na+
KO Na+
WT K+
KO K+
Current amp. (nA)
Potential (mV)
G
Action potential
Threshold
-50 mV
fAHP
10 mV
2 ms
Slope of action potential
0 mV/ms
5 mV/ms
10 mV/ms
H
MAP2 UBE3A
WT
KO
KO+ UBE3A
I
WT
KO
KO+ UBE3A
10 mV
2 ms
J
N.S.
fAHP amplitude(mV)
K
Spike frequency (Hz)
Current (nA)
L
N.S.
Max. spike freq. (Hz)
M
H1 hESC
WT CACCAGTTAA-CTGAGGG
KO CACCAGTTAAACTGAGGG
WT KO
UBE3A
100 kDa
Actin
42 kDa
N
WT (28)
KO (30)
KO + UBE3A (20)
Spike frequency (Hz)
Current (nA)
O
N.S.
Max. spike freq. (Hz)
P
N.S.
fAHP amplitude (mV)
Q
f = a/(1+exp(-(x-x0)/b))
WT
KO
Spike frequency (Hz)
Current (nA)
R
Estimated max. freq. (Hz)
WT KO
S
Estimated half-max. C.i. (nA)
WT KO

Fig. S2. Molecular and functional characterization of human induced neurons.
(**A**) Quantification of $MAP2^+$ neurons derived from WT and KO hESCs. (**B-E**) Quantification of electrophysiological properties of WT and KO neurons. Cm: Capacitance; R_{input}: Input resistance. (**F**) Voltage-gated sodium and potassium channel-mediated current of the induced neurons. (**G**) Representative traces to illustrate spike threshold and fAHP in our patch clamp recordings. Slope of spikes (red) was first calculated, and threshold was defined when slope equals to 5 mV/ms. (**H-J**) Normalization of the excitability and fAHP changes by ectopic expression of UBE3A in KO neurons derived from H9 hESCs. (**H**) Immunostaining for UBE3A(magenta) in WT (H9), KO, and KO neurons expressing UBE3A exogenously. Scale bar: 10 μm. (**I**) representative trace of AP. (**J**) Quantification of spike fAHP amplitude. (**K**) F-I curves showing spike frequency versus current injections in induced neurons. (**L**) Quantification of maximal spike frequency in the current injections. (**M-S**) H1-derived *UBE3A* KO neurons phenocopied neurons derived from H9. (**M**) Schematic illustrating the CRISPR-Cas9-mediated gene editing approach used to knock out *UBE3A* in H1 hESCs (upper) and immunoblot showing the absence of the UBE3A protein in the resultant *UBE3A* KO cells (bottom). (**N**) F-I curves showing spike frequency versus current injections in induced neurons. (**O**) Quantification of maximal spike frequency in the current injections. (**P**) Quantification of spike fAHP amplitude. (**Q-S**) Nonlinear regression sigmoid fitting of F-I curves for induced neurons derived from both H1 (2 batches) and H9 (2 batches) hESCs lines. (**Q**) Sigmoid fitting of F-I curves of induced neurons by formula f(x) using MATLAB toolbox. (**R-S**) Maximal spikes frequency and current injection (C.i.) for half-maximal frequency estimated from the sigmoid. *$P < 0.05$, Two-tailed unpaired Student's t-test was used for J and K. ** $p<0.01$, *$P < 0.05$, Two-tailed paired Student's t-test was used for M and N. In all bars, n indicates the number of analyzed neurons. Data represent mean ± SEM.

Figure S3

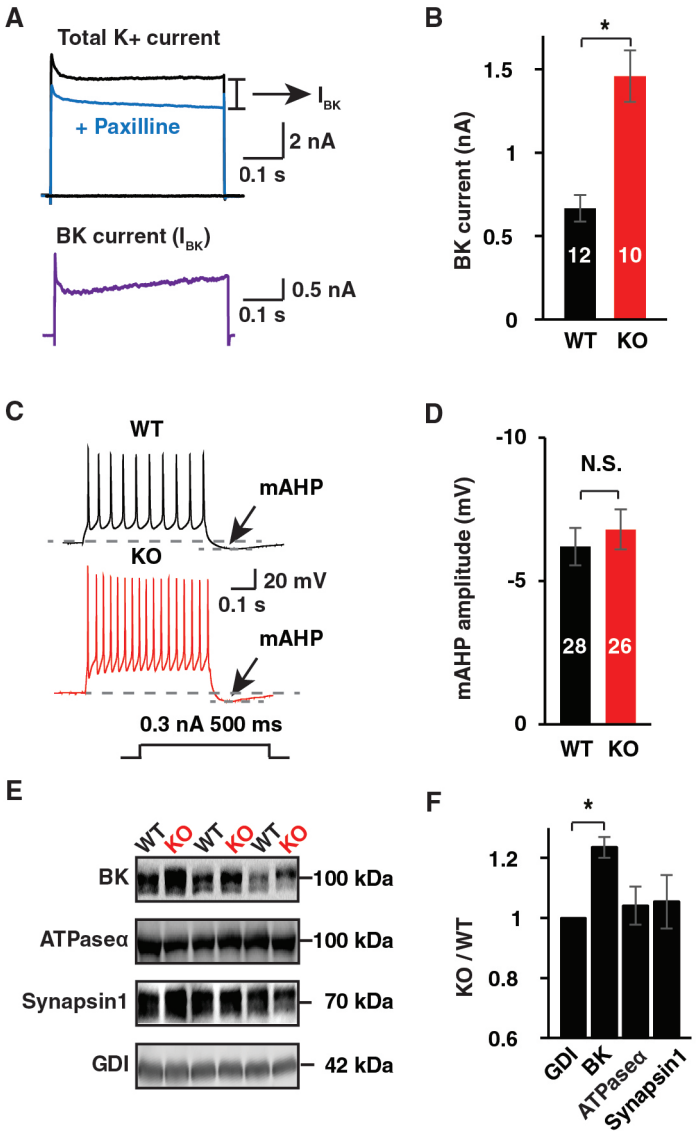

Fig. S3. BK augmentation in human *UBE3A* deficient neurons.
(**A**) Representative traces demonstrating the pharmacological isolation of BK currents following the application of paxilline (5 µM). BK current was calculated by subtracting the evoked current recorded after paxilline treatment from the current evoked before paxilline treatment; voltage clamp recordings were used to perform these experiments. (**B**) Quantification of BK current amplitude in WT and KO neurons. (**C-D**) Representative images and quantification of medium AHP (mAHP) in WT and KO neurons under current injection recordings. (**E**) Representative immunoblotting and (**F**) quantification of protein levels in cell lysates obtained from WT and KO human neurons. N = 3 independent batches of paired WT and KO samples. *P < 0.05, Two-tailed unpaired Student's t-test. N.S. not significant. In all bars, n indicates the number of analyzed neurons. Data represent mean ± SEM.

Figure S4

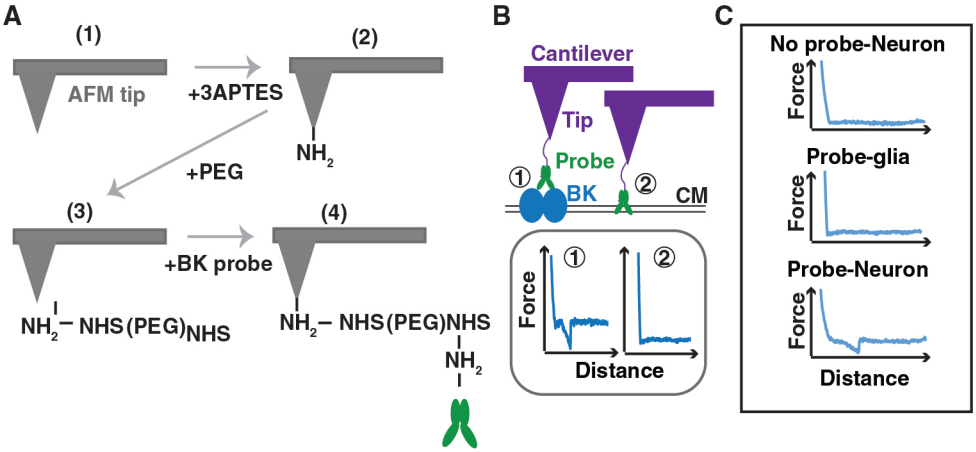

Fig. S4. Schematics illustrating AFM-based BK probing.
(**A**) Schematic of the functionalization of the AFM tip with a BK antibody. (**B**) Diagrams illustrating the detection of BK channels using a functionalized probe with AFM. Force-distance curves obtained in the presence and absence of BK channels. CM: cell membrane. (**C**) Representative force-distance curves observed under the conditions indicated.

Figure S5

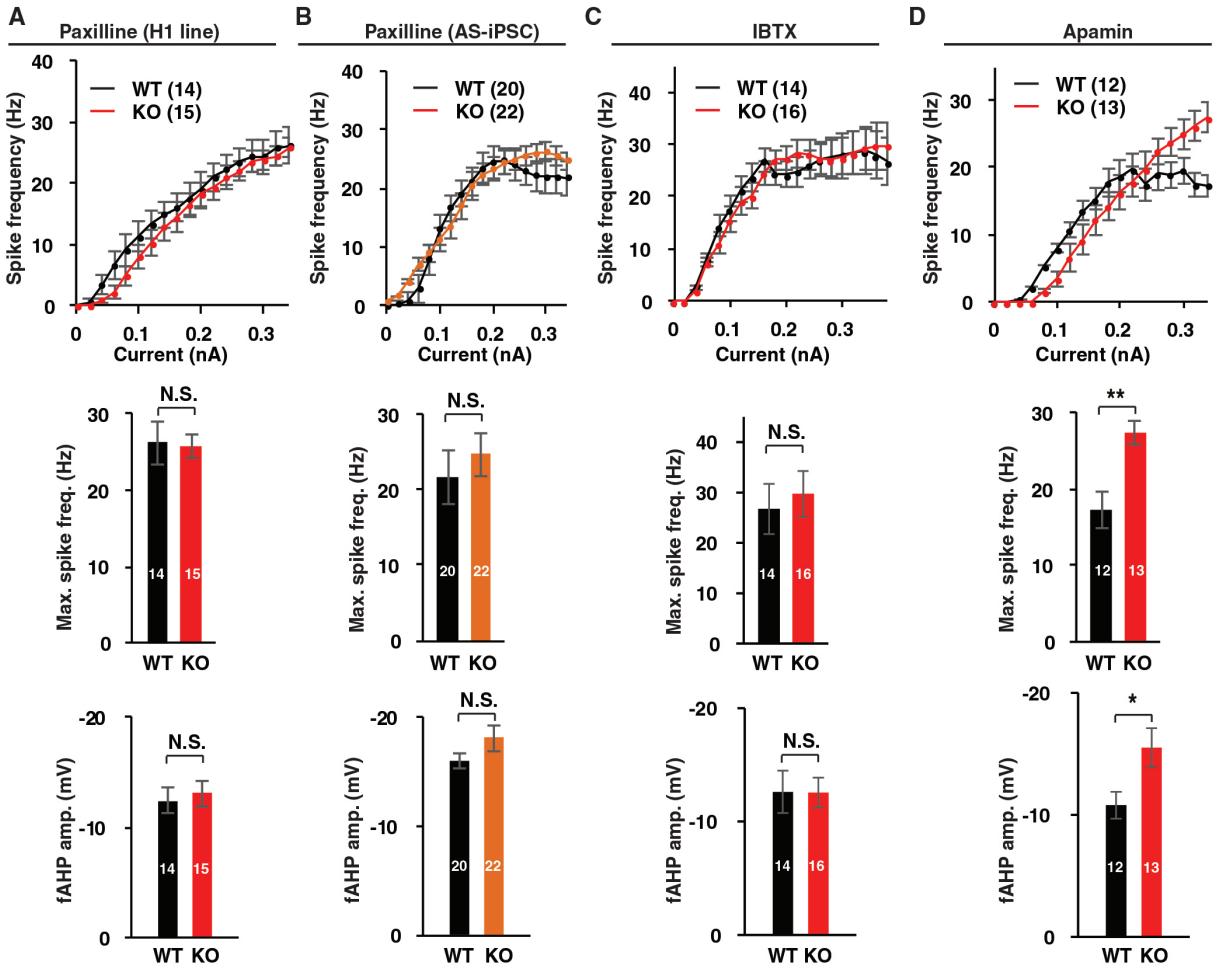

Fig. S5. Additional data on neuronal excitability and fAHP changes in human neurons upon various drug treatments.

Summary of F-I curves, maximum spike frequencies, and fAHP amplitudes with paxilline treatment (5 μM) on neurons induced from (**A**) H1 hESCs, WT and KO; and (**B**) from AS-iPSC line, WT: AS-iPSC+UBE3A; KO, AS-iPSC. WT and UBE3A-KO neurons were treated with (**C**) IBTX (100 nM) and (**D**) apamin (200 nM). ** $p<0.01$, *$P < 0.05$, Two-tailed unpaired Student's t-test. N.S. not significant. In all bars, n indicates the number of analyzed neurons. Data represent mean ± SEM.

Figure S6

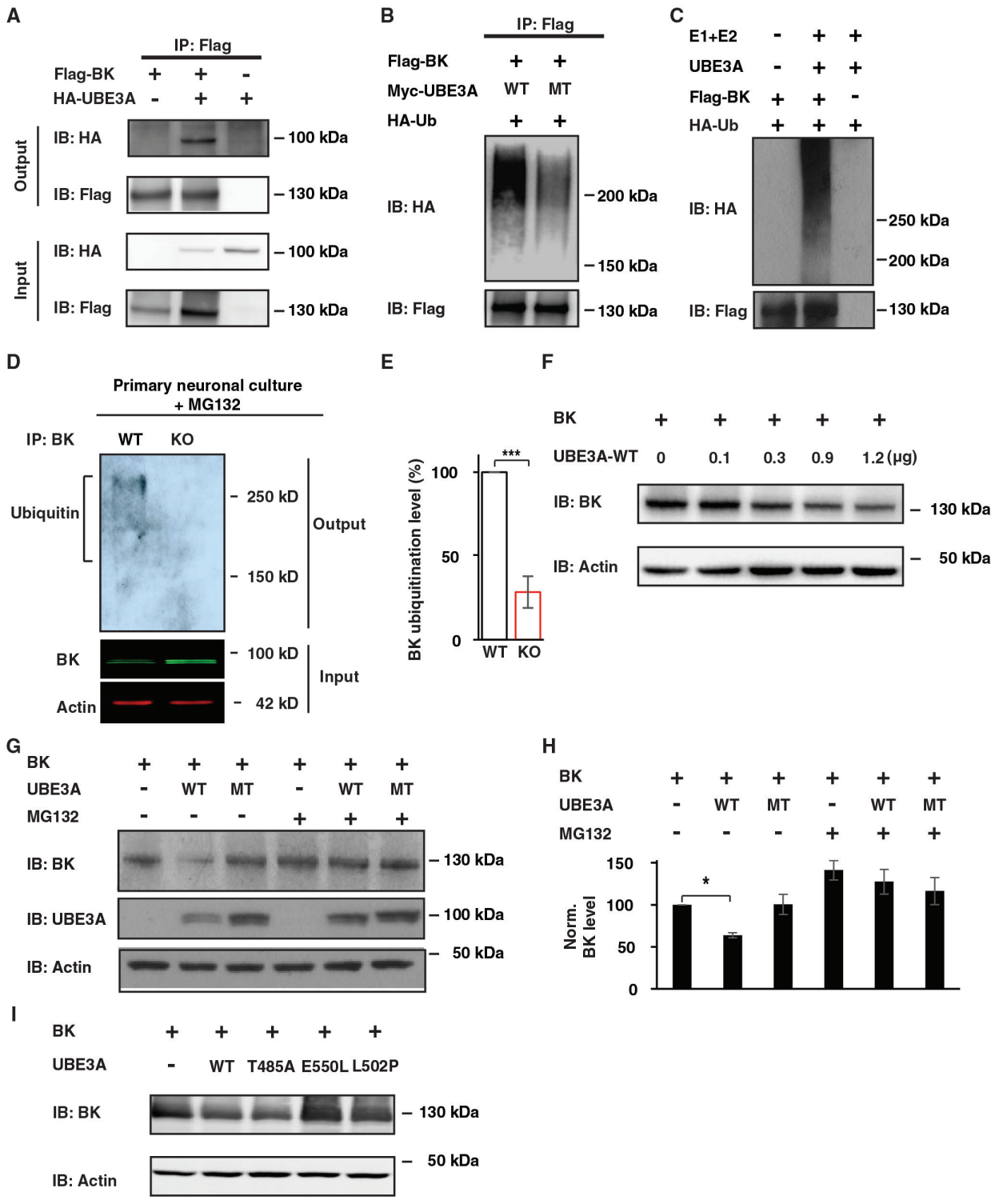
A
IP: Flag
Flag-BK + + -
HA-UBE3A - + +
Output
IB: HA
100 kDa
IB: Flag
130 kDa
Input
IB: HA
100 kDa
IB: Flag
130 kDa
B
IP: Flag
Flag-BK + +
Myc-UBE3A WT MT
HA-Ub + +
IB: HA
200 kDa
150 kDa
IB: Flag
130 kDa
C
E1+E2 - + +
UBE3A - + +
Flag-BK + + -
HA-Ub + + +
IB: HA
250 kDa
200 kDa
IB: Flag
130 kDa
D
Primary neuronal culture
+ MG132
IP: BK WT KO
Ubiquitin
250 kD
150 kD
Output
BK
100 kD
Actin
42 kD
Input
E
***
BK ubiquitination level (%)
100
50
0
WT KO
F
BK + + + + +
UBE3A-WT 0 0.1 0.3 0.9 1.2 (μg)
IB: BK
130 kDa
IB: Actin
50 kDa
G
BK + + + + + +
UBE3A - WT MT - WT MT
MG132 - - - + + +
IB: BK
130 kDa
IB: UBE3A
100 kDa
IB: Actin
50 kDa
H
BK + + + + + +
UBE3A - WT MT - WT MT
MG132 - - - + + +
Norm. BK level
150
100
50
0
*
I
BK + + + + +
UBE3A - WT T485A E550L L502P
IB: BK
130 kDa
IB: Actin
50 kDa

Fig. S6. UBE3A-mediated ubiquitination and degradation of BK.
(**A**) Coimmunoprecipitation assay of BK and UBE3A performed by overexpressing Flag-tagged BK (Flag-BK) and HA-tagged UBE3A (HA-UBE3A) in human embryonic kidney (HEK293) cells. (**B**) Ubiquitination assay of BK performed by coexpressing HA-tagged ubiquitin (HA-Ub) and wildtype (WT) or a catalytically dead mutant of UBE3A (MT, C833A) in HEK293 cells. (**C**) *In vitro* ubiquitination assay of BK and UBE3A. E1: Ube1, E2: UbcH5c, HA-Ub: HA tagged Ubiquitin. (**D-E**) Endogenous BK ubiquination in primary mouse cortical neurons. BK was immunoprecipitated (IP) and BK ubiquitination was detected by Ubiquitin antibody. N=3 batches. Intensity was normalized to WT for each batch. Data represent mean ± SEM. Two-tailed unpaired Student's t-test. *** $p<0.001$. (**F**) Immunoblotting illustrating changes in BK protein levels after exogenous expression of increasing amounts of WT UBE3A in HEK293 cells. WT: wild-type UBE3A. (**G-H**) Representative western blots and quantification of BK levels in HEK293 cells overexpressing WT or MT UBE3A treated with or without MG132 (1 μM). *$P < 0.05$ (one-way ANOVA). (**I**) Immunoblotting illustrating changes in BK protein levels in HEK293 cells overexpressing WT UBE3A or mutants (T485A, E550L, and L502P).

Figure S7

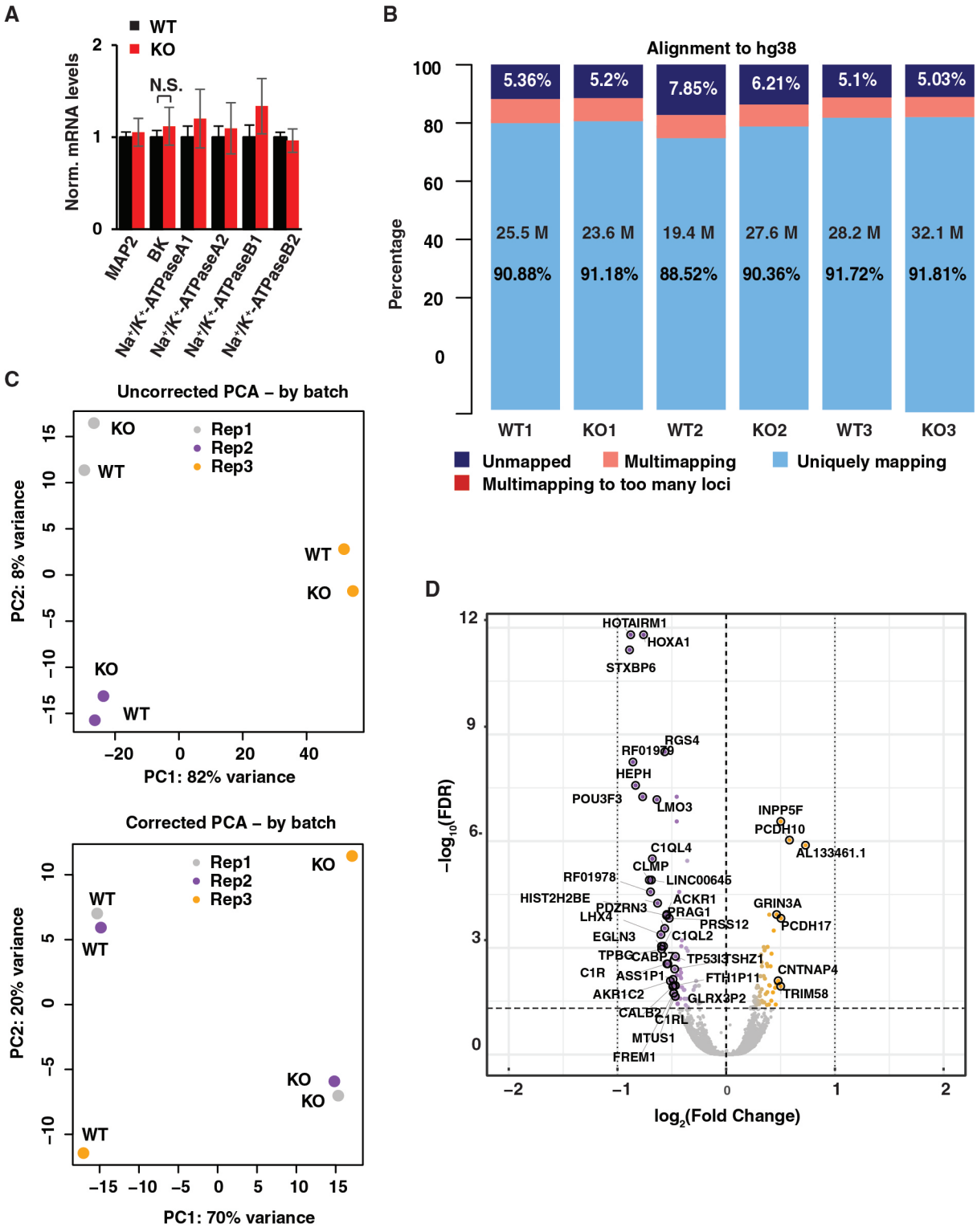
A
WT
KO
N.S.
Norm. mRNA levels
MAP2
BK
Na+/K+-ATPaseA1
Na+/K+-ATPaseA2
Na+/K+-ATPaseB1
Na+/K+-ATPaseB2
B
Alignment to hg38
Percentage
5.36%
5.2%
7.85%
6.21%
5.1%
5.03%
25.5 M
90.88%
23.6 M
91.18%
19.4 M
88.52%
27.6 M
90.36%
28.2 M
91.72%
32.1 M
91.81%
WT1
KO1
WT2
KO2
WT3
KO3
Unmapped
Multimapping
Uniquely mapping
Multimapping to too many loci
C
Uncorrected PCA – by batch
Rep1
Rep2
Rep3
PC2: 8% variance
PC1: 82% variance
Corrected PCA – by batch
PC2: 20% variance
PC1: 70% variance
D
HOTAIRM1
HOXA1
STXBP6
RGS4
RF01978
HEPH
POU3F3
LMO3
INPP5F
PCDH10
AL133461.1
C1QL4
CLMP
LINC00645
HIST2H2BE
ACKR1
PDZRN3
PRAG1
GRIN3A
LHX4
PRSS12
PCDH17
EGLN3
C1QL2
TPBG
CABP7
TP53I3
TSHZ1
C1R
ASS1P1
FTH1P11
CNTNAP4
AKR1C2
GLRX3P2
TRIM58
CALB2
C1RL
MTUS1
FREM1
−log10(FDR)
log2(Fold Change)

Fig. S7. qPCR and RNA-sequencing analyses of human induced neurons.
(**A**) Quantification of mRNA levels of channel genes based on quantitative RT-PCR. N = 4 independent batches of samples. Data represent mean ± SEM. (**B)** Quality control of RNA-seq libraries. Percentages and absolute quantities of reads uniquely mapped to the human genome after the removal of rat reads. M=Millions of reads. (**C**) Principal component analysis (PCA) performed before and after batch effects were modeled, showing clustering by genotype along the first principal component (PC1) after correction. (**D**) Volcano plot showing the differential expression analysis of *UBE3A* KO vs WT RNA-seq data. FDR: False discovery rate-adjusted p-value.

Figure S8

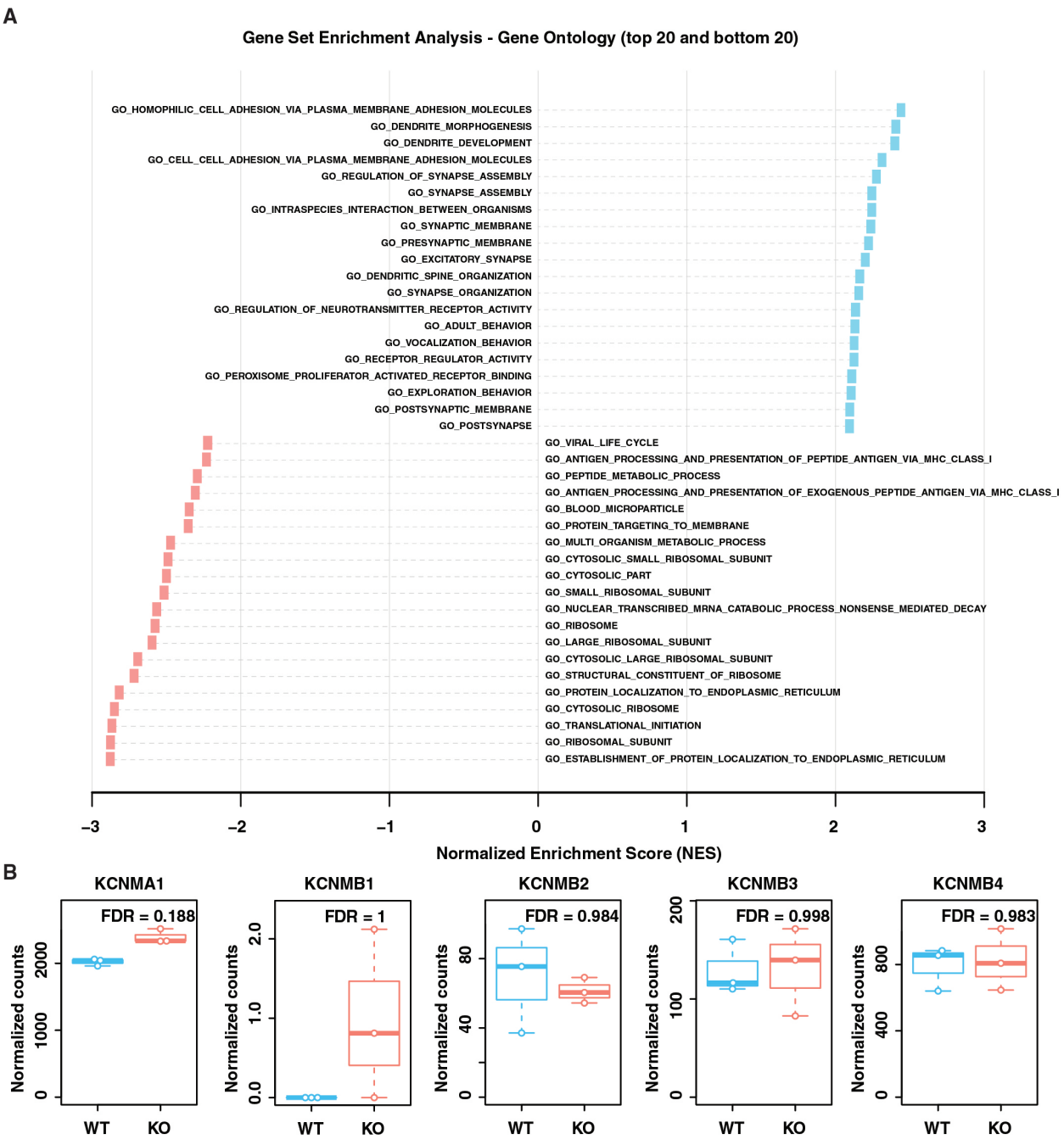

Fig. S8. RNA sequencing analyses of human induced neurons.
(**A**) Gene set enrichment analysis for Gene Ontology categories using DEGs between KO and WT induced neurons. (**B**) Normalized read counts for BK channel related genes: KCNMA1 for BKα, KCNMB1 for BKβ1, KCNMB2 for BKβ2, KCNMB3 for BKβ3, and KCNMB4 for BKβ4. FDR=False Discovery Rate-adjusted p-value for differential expression.

Figure S9

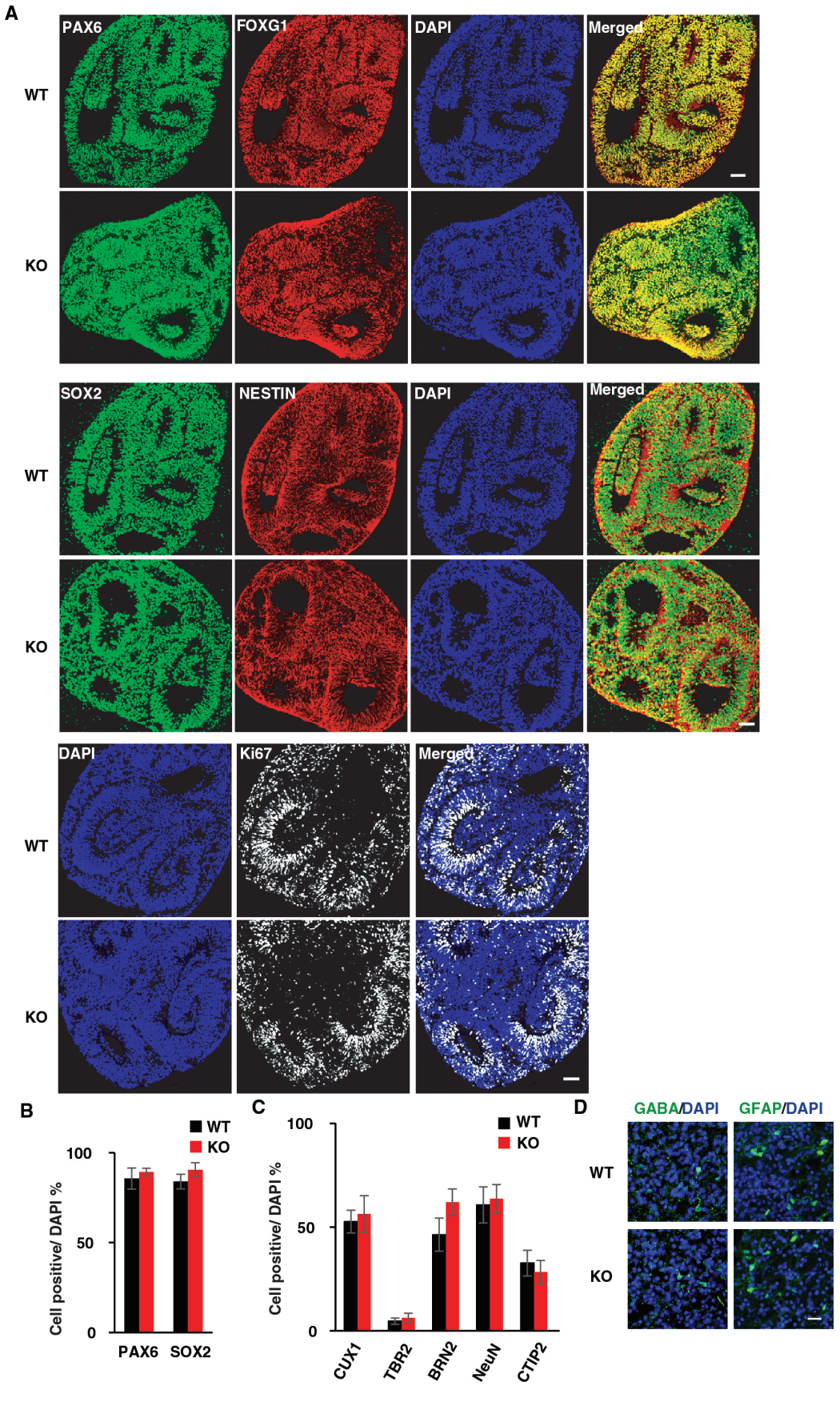
A
PAX6
FOXG1
DAPI
Merged
WT
KO
SOX2
NESTIN
DAPI
Merged
WT
KO
DAPI
Ki67
Merged
WT
KO
B
WT
KO
100
50
0
Cell positive/ DAPI %
PAX6
SOX2
C
WT
KO
100
50
0
Cell positive/ DAPI %
CUX1
TBR2
BRN2
NeuN
CTIP2
D
GABA/DAPI
GFAP/DAPI
WT
KO

Fig. S9. Characterization of human cortical organoids.
(**A-B**) Representative images of immunostaining with neural progenitor markers and quantification in WT and KO organoids on day 20. Scale bar: 80 µm. (**C**) Quantification of cortical neuron markers in WT and KO organoids on day 120. Data represent mean ± SEM. (**D**) Representative images of organoids immunostained with antibodies against GABA and GFAP. Scale bar: 20 µm.

Figure S10

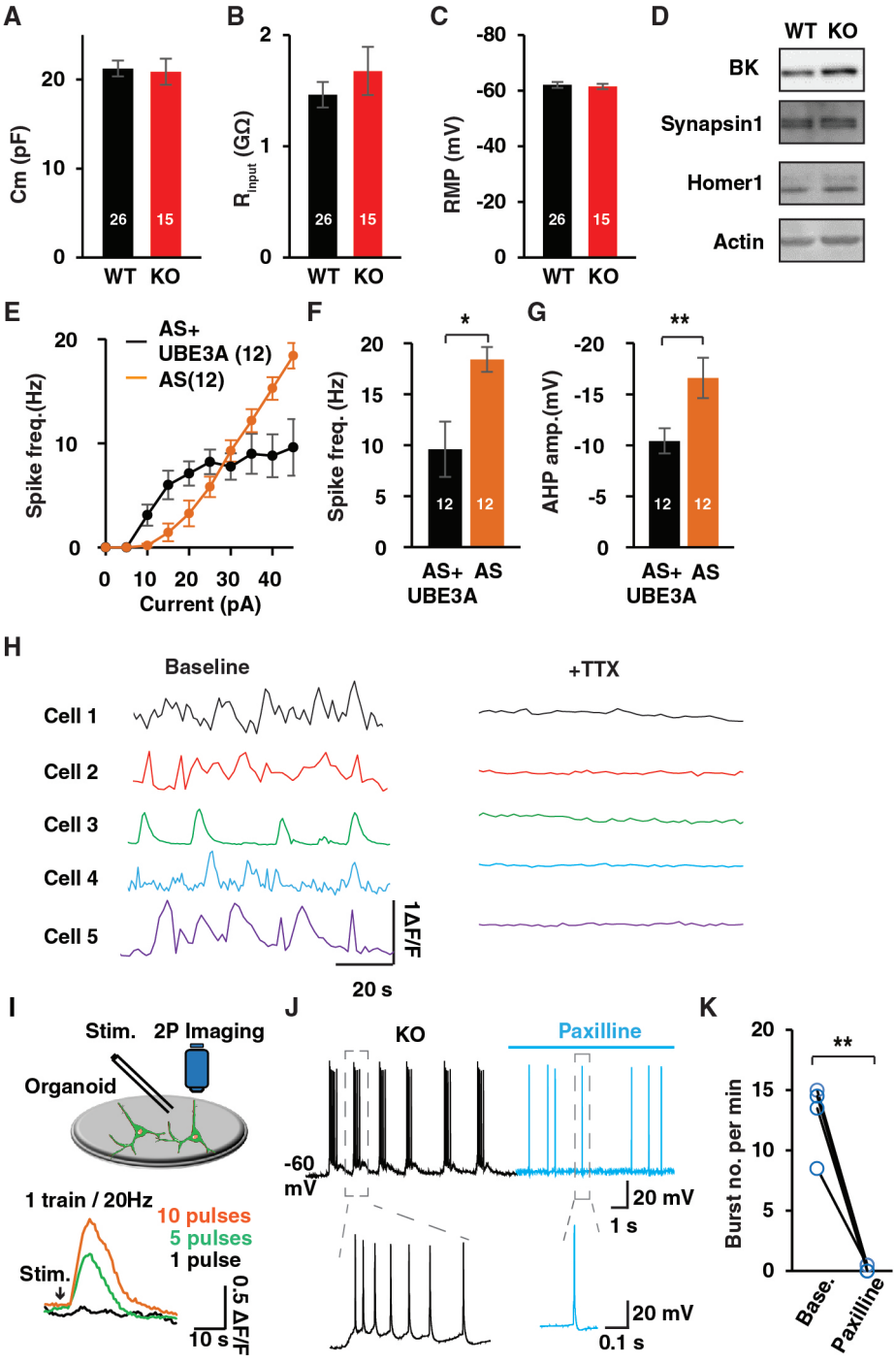
A
Cm (pF)
20
10
0
26
15
WT KO
B
R_{input} (GΩ)
2
1
0
26
15
WT KO
C
RMP (mV)
-80
-60
-40
-20
0
26
15
WT KO
D
WT KO
BK
Synapsin1
Homer1
Actin
E
Spike freq.(Hz)
AS+ UBE3A (12)
AS(12)
0 10 20 30 40
Current (pA)
F
Spike freq. (Hz)
*
12 12
AS+ AS
UBE3A
G
AHP amp.(mV)
**
12 12
AS+ AS
UBE3A
H
Baseline
+TTX
Cell 1
Cell 2
Cell 3
Cell 4
Cell 5
1ΔF/F
20 s
I
Stim. 2P Imaging
Organoid
1 train / 20Hz
10 pulses
5 pulses
1 pulse
Stim.
0.5 ΔF/F
10 s
J
KO
Paxilline
-60 mV
20 mV
1 s
20 mV
0.1 s
K
Burst no. per min
**
Base.
Paxilline

Fig. S10. Functional characterization of brain organoids derived from WT, KO, and AS-iPSCs.
(**A-C**) Quantification of electrophysiological properties of neurons in the organoids. C_m: Capacitance; R_{input}: input resistance; RMP: resting membrane potential. (**D**) Immunoblotting of BK protein and other neuronal markers in WT and UBE3A-KO organoids. (**E-G**) F-I curve and quantification of spike frequencies and fAHP amplitudes in organoid neurons generated from AS-iPSCs and AS-iPSCs overexpressing UBE3A. (**H**) Spontaneous calcium spikes before and after TTX treatment (2 μM). **P < 0.01, *P < 0.05, Two-tailed paired Student's t-test was used for all panels. (**I**) Calcium transients evoked by graded electrical trains-stimuli (Stim.) and recorded by 2P imaging. (**J**) Representative traces of spontaneous spikes observed in perforated patch clamp recordings obtained from KO organoids before and after paxilline treatment (10 μM). (**K**) Quantification of spontaneous burst frequencies observed before and after paxilline treatment. Spike trains with more than 4 spikes were considered as bursts. N = 4 organoids. Data represent mean ± SEM.

Figure S11

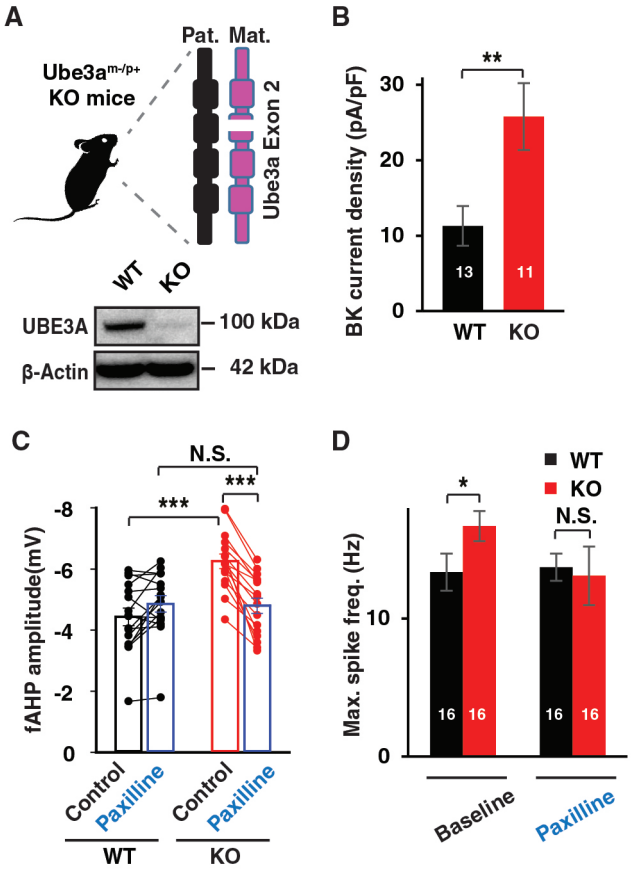

Fig. S11. BK augmentation and increased fAHP in neurons of *Ube3a*$^{m-/p+}$ mice.
(**A**) Schematic of *Ube3a* deletion in the maternal allele in *Ube3a*$^{m-/p+}$ mice (top) and Ube3a loss confirmed by immunoblotting (bottom). (**B**) BK current isolated from acute hippocampal slices of WT and KO mice by paxilline (10 μM). Quantifications of fAHP amplitudes (**C**) and maximal spike frequency with current injections (**D**) of recorded mouse neurons. In all bars, n indicates the number of analyzed neurons. Data represent mean ± SEM.

Figure S12

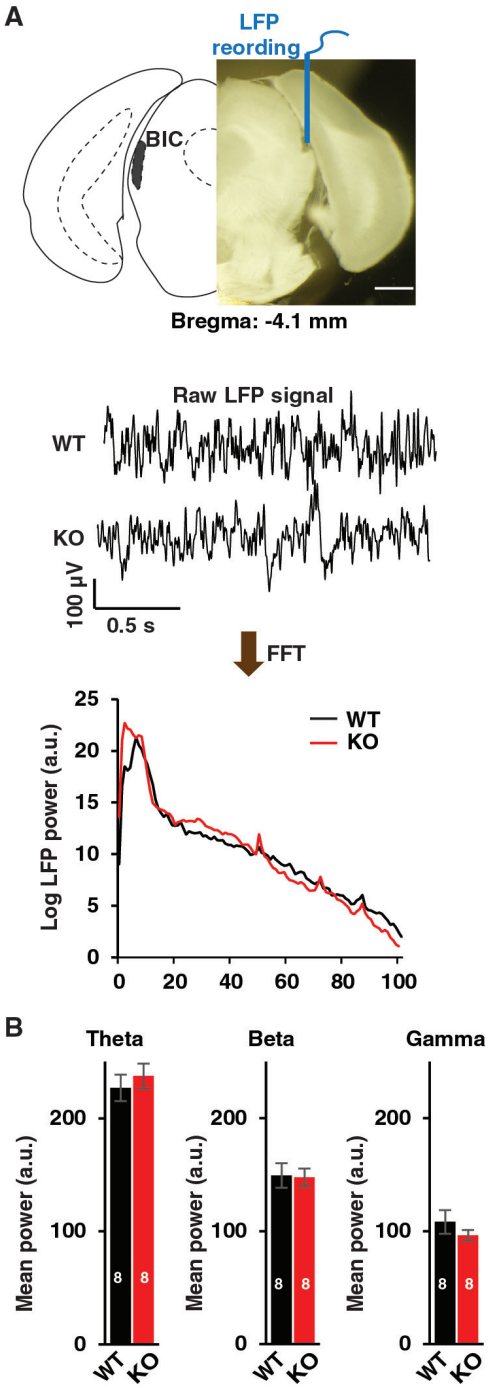

Fig. S12. LFP recordings in the brain of WT and *Ube3a*$^{m-/p+}$ mice.
(**A**) Schematic of local field potential (LFP) recording in the brachium of inferior colliculus (BIC) with audio stimuli (~125 dB). Raw LFPs (mid) were recorded by sampling at 500 Hz, filtered with 0.5 Hz high-pass and 100 Hz low-pass, and then analyzed by fast Fourier transform (FFT) for power spectral density (PSD). (**B**) Quantification of different rhythmicity power of LFP recorded from WT and *Ube3a*$^{m-/p+}$ mice. Theta: 4-8 Hz; Beta: 12-30 Hz; Gamma: 30-80 Hz. Data represent mean ± SEM.

Figure S13

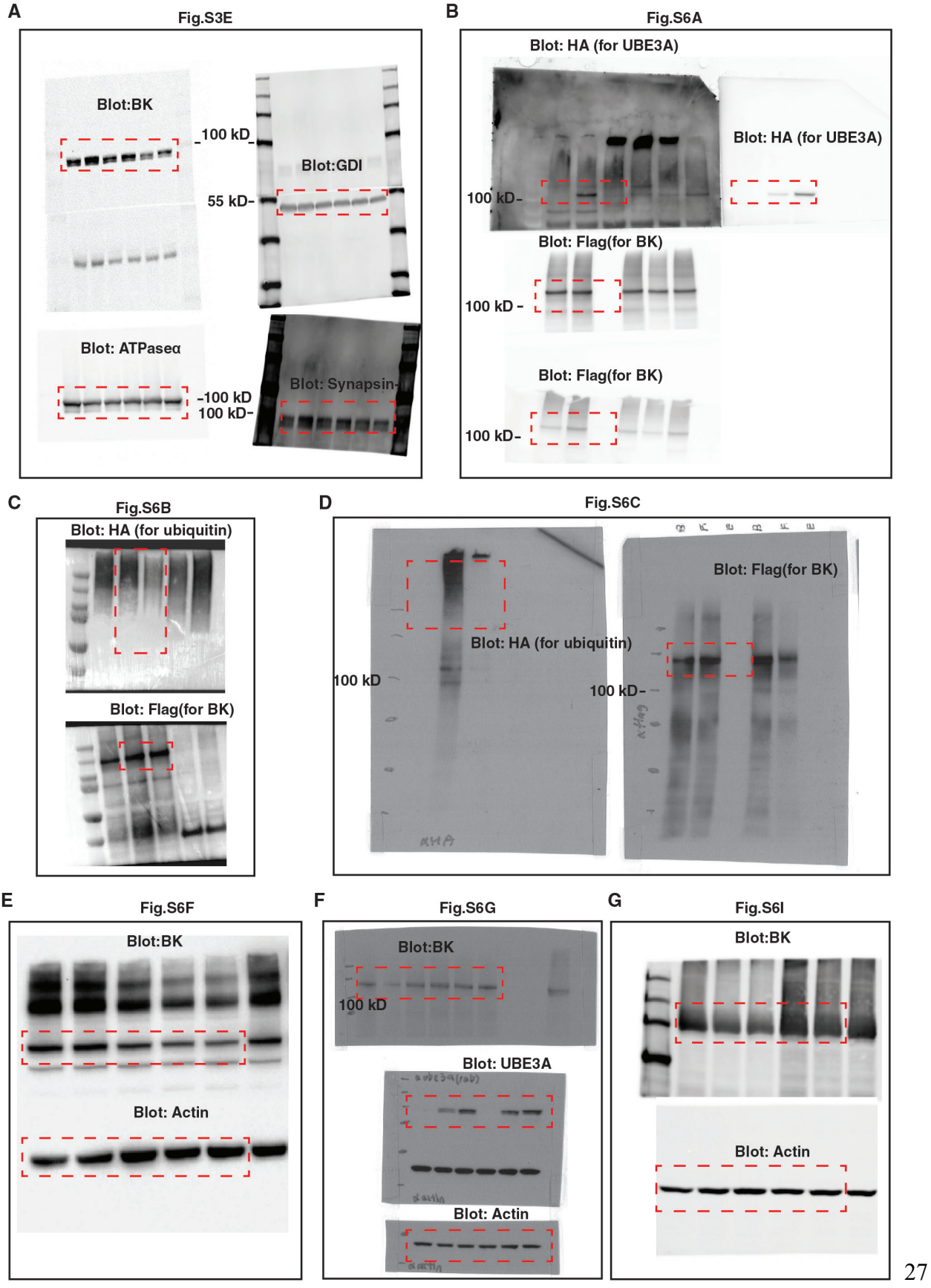
A
Fig.S3E
Blot:BK
100 kD
Blot:GDI
55 kD
Blot: ATPaseα
100 kD
100 kD
Blot: Synapsin
B
Fig.S6A
Blot: HA (for UBE3A)
Blot: HA (for UBE3A)
100 kD
Blot: Flag(for BK)
100 kD
Blot: Flag(for BK)
100 kD
C
Fig.S6B
Blot: HA (for ubiquitin)
Blot: Flag(for BK)
D
Fig.S6C
Blot: HA (for ubiquitin)
100 kD
Blot: Flag(for BK)
100 kD
E
Fig.S6F
Blot:BK
Blot: Actin
F
Fig.S6G
Blot:BK
100 kD
Blot: UBE3A
Blot: Actin
G
Fig.S6I
Blot:BK
Blot: Actin

Fig. S13. Full-length Western blot images. (**A**) Full-length blot image for Fig. S3E. (**B**) Full-length blot image for Fig. S6A. (**C**) Full-length blot image for Fig. S6B. (**D**) Full-length blot image for Fig. S6C. (**E**) Full-length blot image for Fig. S6F. (**F**) Full-length blot image for Fig. S6G. (**G**) Full-length blot image for Fig. S6I.

Movie S1. Volumetric imaging of a WT cortical organoid stained with Fluo-4 AM.

Movie S2. Spontaneous calcium (Ca^{2+}) transient activities within a cortical organoid before and after TTX treatment.

Movie S3. Spontaneous Ca^{2+} transient activities in neurons within cortical organoids derived from either WT or UBE3A KO hESCs.

Movie S4. Spontaneous Ca^{2+} transient activities in neurons within a cortical organoids derived from AS patient-derived iPSCs.

Table S1. List of top 10 potential CRISPR-Cas9 off-target loci

Table S2. Results of the differential gene expression analysis

Table S3. Results of the Gene Set Enrichment Analysis - GO Collection

Table S4. Results of the Gene Ontology and KEGG Pathway over-representation analysis

Table S5. qPCR primer sequences

References and Notes

1. K. Buiting, C. Williams, B. Horsthemke, Angelman syndrome—insights into a rare neurogenetic disorder. *Nat. Rev. Neurol.* **12**, 584–593 (2016). doi:10.1038/nrneurol.2016.133 Medline

2. A. M. Mabb, M. C. Judson, M. J. Zylka, B. D. Philpot, Angelman syndrome: Insights into genomic imprinting and neurodevelopmental phenotypes. *Trends Neurosci.* **34**, 293–303 (2011). doi:10.1016/j.tins.2011.04.001 Medline

3. G. L. Sell, S. S. Margolis, From UBE3A to Angelman syndrome: A substrate perspective. *Front. Neurosci.* **9**, 322 (2015). doi:10.3389/fnins.2015.00322 Medline

4. Y. H. Jiang, D. Armstrong, U. Albrecht, C. M. Atkins, J. L. Noebels, G. Eichele, J. D. Sweatt, A. L. Beaudet, Mutation of the Angelman ubiquitin ligase in mice causes increased cytoplasmic p53 and deficits of contextual learning and long-term potentiation. *Neuron* **21**, 799–811 (1998). doi:10.1016/S0896-6273(00)80596-6 Medline

5. M. L. Wallace, A. C. Burette, R. J. Weinberg, B. D. Philpot, Maternal loss of Ube3a produces an excitatory/inhibitory imbalance through neuron type-specific synaptic defects. *Neuron* **74**, 793–800 (2012). doi:10.1016/j.neuron.2012.03.036 Medline

6. M. L. Wallace, G. M. van Woerden, Y. Elgersma, S. L. Smith, B. D. Philpot, *Ube3a* loss increases excitability and blunts orientation tuning in the visual cortex of Angelman syndrome model mice. *J. Neurophysiol.* **118**, 634–646 (2017). doi:10.1152/jn.00618.2016 Medline

7. M. C. Judson, M. L. Wallace, M. S. Sidorov, A. C. Burette, B. Gu, G. M. van Woerden, I. F. King, J. E. Han, M. J. Zylka, Y. Elgersma, R. J. Weinberg, B. D. Philpot, GABAergic Neuron-Specific Loss of Ube3a Causes Angelman Syndrome-Like EEG Abnormalities and Enhances Seizure Susceptibility. *Neuron* **90**, 56–69 (2016). doi:10.1016/j.neuron.2016.02.040 Medline

8. M. C. Judson, A. C. Burette, C. L. Thaxton, A. L. Pribisko, M. D. Shen, A. M. Rumple, W. A. Del Cid, B. Paniagua, M. Styner, R. J. Weinberg, B. D. Philpot, Decreased Axon Caliber Underlies Loss of Fiber Tract Integrity, Disproportional Reductions in White Matter Volume, and Microcephaly in Angelman Syndrome Model Mice. *J. Neurosci.* **37**, 7347–7361 (2017). doi:10.1523/JNEUROSCI.0037-17.2017 Medline

9. S. J. Chamberlain, P.-F. Chen, K. Y. Ng, F. Bourgois-Rocha, F. Lemtiri-Chlieh, E. S. Levine, M. Lalande, Induced pluripotent stem cell models of the genomic imprinting disorders Angelman and Prader-Willi syndromes. *Proc. Natl. Acad. Sci. U.S.A.* **107**, 17668–17673 (2010). doi:10.1073/pnas.1004487107 Medline

10. J. J. Fink, T. M. Robinson, N. D. Germain, C. L. Sirois, K. A. Bolduc, A. J. Ward, F. Rigo, S. J. Chamberlain, E. S. Levine, Disrupted neuronal maturation in Angelman syndrome-derived induced pluripotent stem cells. *Nat. Commun.* **8**, 15038 (2017). doi:10.1038/ncomms15038 Medline

11. Y. Zhang, C. Pak, Y. Han, H. Ahlenius, Z. Zhang, S. Chanda, S. Marro, C. Patzke, C. Acuna, J. Covy, W. Xu, N. Yang, T. Danko, L. Chen, M. Wernig, T. C. Südhof, Rapid single-

step induction of functional neurons from human pluripotent stem cells. *Neuron* **78**, 785–798 (2013). doi:10.1016/j.neuron.2013.05.029 Medline

12. F. Yi, T. Danko, S. C. Botelho, C. Patzke, C. Pak, M. Wernig, T. C. Südhof, Autism-associated SHANK3 haploinsufficiency causes I_h channelopathy in human neurons. *Science* **352**, aaf2669 (2016). doi:10.1126/science.aaf2669 Medline

13. B. P. Bean, The action potential in mammalian central neurons. *Nat. Rev. Neurosci.* **8**, 451–465 (2007). doi:10.1038/nrn2148 Medline

14. N. Gu, K. Vervaeke, J. F. Storm, BK potassium channels facilitate high-frequency firing and cause early spike frequency adaptation in rat CA1 hippocampal pyramidal cells. *J. Physiol.* **580**, 859–882 (2007). doi:10.1113/jphysiol.2006.126367 Medline

15. J. R. Montgomery, A. L. Meredith, Genetic activation of BK currents in vivo generates bidirectional effects on neuronal excitability. *Proc. Natl. Acad. Sci. U.S.A.* **109**, 18997–19002 (2012). doi:10.1073/pnas.1205573109 Medline

16. T. Kimm, Z. M. Khaliq, B. P. Bean, Differential Regulation of Action Potential Shape and Burst-Frequency Firing by BK and Kv2 Channels in Substantia Nigra Dopaminergic Neurons. *J. Neurosci.* **35**, 16404–16417 (2015). doi:10.1523/JNEUROSCI.5291-14.2015 Medline

17. J. F. Storm, Action potential repolarization and a fast after-hyperpolarization in rat hippocampal pyramidal cells. *J. Physiol.* **385**, 733–759 (1987). doi:10.1113/jphysiol.1987.sp016517 Medline

18. J. Sun, G. Zhu, Y. Liu, S. Standley, A. Ji, R. Tunuguntla, Y. Wang, C. Claus, Y. Luo, M. Baudry, X. Bi, UBE3A Regulates Synaptic Plasticity and Learning and Memory by Controlling SK2 Channel Endocytosis. *Cell Rep.* **12**, 449–461 (2015). doi:10.1016/j.celrep.2015.06.023 Medline

19. J. L. Maciaszek, H. Soh, R. S. Walikonis, A. V. Tzingounis, G. Lykotrafitis, Topography of native SK channels revealed by force nanoscopy in living neurons. *J. Neurosci.* **32**, 11435–11440 (2012). doi:10.1523/JNEUROSCI.1785-12.2012 Medline

20. B. Sadikovic, P. Fernandes, V. W. Zhang, P. A. Ward, I. Miloslavskaya, W. Rhead, R. Rosenbaum, R. Gin, B. Roa, P. Fang, Mutation Update for UBE3A variants in Angelman syndrome. *Hum. Mutat.* **35**, 1407–1417 (2014). doi:10.1002/humu.22687 Medline

21. J. J. Yi, S. R. Paranjape, M. P. Walker, R. Choudhury, J. M. Wolter, G. Fragola, M. J. Emanuele, M. B. Major, M. J. Zylka, The autism-linked UBE3A T485A mutant E3 ubiquitin ligase activates the Wnt/β-catenin pathway by inhibiting the proteasome. *J. Biol. Chem.* **292**, 12503–12515 (2017). doi:10.1074/jbc.M117.788448 Medline

22. S. Ramamoorthy, Z. Nawaz, E6-associated protein (E6-AP) is a dual function coactivator of steroid hormone receptors. *Nucl. Recept. Signal.* **6**, e006 (2008). doi:10.1621/nrs.06006 Medline

23. A. M. Paşca, S. A. Sloan, L. E. Clarke, Y. Tian, C. D. Makinson, N. Huber, C. H. Kim, J.-Y. Park, N. A. O'Rourke, K. D. Nguyen, S. J. Smith, J. R. Huguenard, D. H. Geschwind, B. A. Barres, S. P. Paşca, Functional cortical neurons and astrocytes from human pluripotent

stem cells in 3D culture. *Nat. Methods* **12**, 671–678 (2015). doi:10.1038/nmeth.3415 Medline

24. I. Kelava, M. A. Lancaster, Stem Cell Models of Human Brain Development. *Cell Stem Cell* **18**, 736–748 (2016). doi:10.1016/j.stem.2016.05.022 Medline

25. P. Kirwan, B. Turner-Bridger, M. Peter, A. Momoh, D. Arambepola, H. P. C. Robinson, F. J. Livesey, Development and function of human cerebral cortex neural networks from pluripotent stem cells in vitro. *Development* **142**, 3178–3187 (2015). doi:10.1242/dev.123851 Medline

26. J. N. Kerr, D. Greenberg, F. Helmchen, Imaging input and output of neocortical networks in vivo. *Proc. Natl. Acad. Sci. U.S.A.* **102**, 14063–14068 (2005). doi:10.1073/pnas.0506029102 Medline

27. V. Emiliani, A. E. Cohen, K. Deisseroth, M. Häusser, All-Optical Interrogation of Neural Circuits. *J. Neurosci.* **35**, 13917–13926 (2015). doi:10.1523/JNEUROSCI.2916-15.2015 Medline

28. K. Pelc, S. G. Boyd, G. Cheron, B. Dan, Epilepsy in Angelman syndrome. *Seizure* **17**, 211–217 (2008). doi:10.1016/j.seizure.2007.08.004 Medline

29. Y. Jiang, T. F. Tsai, J. Bressler, A. L. Beaudet, Imprinting in Angelman and Prader-Willi syndromes. *Curr. Opin. Genet. Dev.* **8**, 334–342 (1998). doi:10.1016/S0959-437X(98)80091-9 Medline

30. R. J. Racine, Modification of seizure activity by electrical stimulation. II. Motor seizure. *Electroencephalogr. Clin. Neurophysiol.* **32**, 281–294 (1972). doi:10.1016/0013-4694(72)90177-0 Medline

31. M. S. Sidorov, G. M. Deck, M. Dolatshahi, R. L. Thibert, L. M. Bird, C. J. Chu, B. D. Philpot, Delta rhythmicity is a reliable EEG biomarker in Angelman syndrome: A parallel mouse and human analysis. *J. Neurodev. Disord.* **9**, 17 (2017). doi:10.1186/s11689-017-9195-8 Medline

32. N. E. Sanjana, O. Shalem, F. Zhang, Improved vectors and genome-wide libraries for CRISPR screening. *Nat. Methods* **11**, 783–784 (2014). doi:10.1038/nmeth.3047 Medline

33. A. X. Sun, Q. Yuan, S. Tan, Y. Xiao, D. Wang, A. T. T. Khoo, L. Sani, H.-D. Tran, P. Kim, Y. S. Chiew, K. J. Lee, Y.-C. Yen, H. H. Ng, B. Lim, H. S. Je, Direct Induction and Functional Maturation of Forebrain GABAergic Neurons from Human Pluripotent Stem Cells. *Cell Rep.* **16**, 1942–1953 (2016). doi:10.1016/j.celrep.2016.07.035 Medline

34. J. Platkiewicz, R. Brette, A threshold equation for action potential initiation. *PLOS Comput. Biol.* **6**, e1000850 (2010). doi:10.1371/journal.pcbi.1000850 Medline

35. Y. Yu, Y. Shu, D. A. McCormick, Cortical action potential backpropagation explains spike threshold variability and rapid-onset kinetics. *J. Neurosci.* **28**, 7260–7272 (2008). doi:10.1523/JNEUROSCI.1613-08.2008 Medline

36. A. Li, T. S. Lim, H. Shi, J. Yin, S. J. Tan, Z. Li, B. C. Low, K. S. W. Tan, C. T. Lim, Molecular mechanistic insights into the endothelial receptor mediated cytoadherence of Plasmodium falciparum-infected erythrocytes. *PLOS ONE* **6**, e16929 (2011). doi:10.1371/journal.pone.0016929 Medline

37. Y. B. Lim, J. Thingna, J. Cao, C. T. Lim, Single molecule and multiple bond characterization of catch bond associated cytoadhesion in malaria. *Sci. Rep.* **7**, 4208 (2017). doi:10.1038/s41598-017-04352-x Medline

38. T. Conway, J. Wazny, A. Bromage, M. Tymms, D. Sooraj, E. D. Williams, B. Beresford-Smith, Xenome—A tool for classifying reads from xenograft samples. *Bioinformatics* **28**, i172–i178 (2012). doi:10.1093/bioinformatics/bts236 Medline

39. A. Dobin, C. A. Davis, F. Schlesinger, J. Drenkow, C. Zaleski, S. Jha, P. Batut, M. Chaisson, T. R. Gingeras, STAR: Ultrafast universal RNA-seq aligner. *Bioinformatics* **29**, 15–21 (2013). doi:10.1093/bioinformatics/bts635 Medline

40. Y. Liao, G. K. Smyth, W. Shi, The Subread aligner: Fast, accurate and scalable read mapping by seed-and-vote. *Nucleic Acids Res.* **41**, e108 (2013). doi:10.1093/nar/gkt214 Medline

41. J. T. Leek, W. E. Johnson, H. S. Parker, A. E. Jaffe, J. D. Storey, The sva package for removing batch effects and other unwanted variation in high-throughput experiments. *Bioinformatics* **28**, 882–883 (2012). doi:10.1093/bioinformatics/bts034 Medline

42. J. T. Leek, J. D. Storey, A general framework for multiple testing dependence. *Proc. Natl. Acad. Sci. U.S.A.* **105**, 18718–18723 (2008). doi:10.1073/pnas.0808709105 Medline

43. M. I. Love, W. Huber, S. Anders, Moderated estimation of fold change and dispersion for RNA-seq data with DESeq2. *Genome Biol.* **15**, 550 (2014). doi:10.1186/s13059-014-0550-8 Medline

44. J. Reimand, T. Arak, P. Adler, L. Kolberg, S. Reisberg, H. Peterson, J. Vilo, g:Profiler-a web server for functional interpretation of gene lists (2016 update). *Nucleic Acids Res.* **44**, W83–W89 (2016). doi:10.1093/nar/gkw199 Medline

45. A. Subramanian, P. Tamayo, V. K. Mootha, S. Mukherjee, B. L. Ebert, M. A. Gillette, A. Paulovich, S. L. Pomeroy, T. R. Golub, E. S. Lander, J. P. Mesirov, Gene set enrichment analysis: A knowledge-based approach for interpreting genome-wide expression profiles. *Proc. Natl. Acad. Sci. U.S.A.* **102**, 15545–15550 (2005). doi:10.1073/pnas.0506580102 Medline

46. A. Liberzon, A. Subramanian, R. Pinchback, H. Thorvaldsdóttir, P. Tamayo, J. P. Mesirov, Molecular signatures database (MSigDB) 3.0. *Bioinformatics* **27**, 1739–1740 (2011). doi:10.1093/bioinformatics/btr260 Medline

47. A. Sergushichev, An algorithm for fast preranked gene set enrichment analysis using cumulative statistic calculation. bioRxiv 060012 [Preprint]. 20 June 2016. https://doi.org/10.1101/060012.